SCIENTIFIC REPORTS
nature research

Check for updates

OPEN

The kinetics and mechanism of the uranium hydride - water vapour system under ambient conditions

A. Banos✉ & T. B. Scott

This work investigated the reaction of uranium hydride powder with saturated water vapour at 25 °C. Two corrosion experiments were conducted one with deionised water (H_2O) and one with deuterated water (D_2O). The kinetics of the reaction were measured through gas generation method while concurrent residual gas analysis (RGA) allowed better understanding of the oxidation mechanism governing the system. From the analysis, it was found that the kinetics of the reaction are robust initially, followed by quasi-linear decelerating regime indicative of a 'shrinking core' type oxidation behaviour. The extent of the reaction (conversion to UO_2) was lower in comparison to other works. The reaction remained incomplete bolstering the case of UH_3 persistence in legacy wastes. Through interpretation of the gas analysis data, a mechanism for the uranium hydride water reaction was suggested.

The Sellafield legacy ponds and silos consist of four plants which were historically used for the interim storage of unconditioned waste awaiting to be reprocessed or prepared for long-term storage and disposal[1,2]. Intermediate level waste (ILW), mainly comprised of uranium-contaminated materials like Magnox cladding, etc. and radioactive sludge have been accumulated in these plants for over six decades to keep them safely isolated from the environment[1,3]. Under a water environment uranium oxidises to produce uranium dioxide (UO_2), and H_2 gas (Eq. 1). In an enclosed environment, H_2 can be trapped in the vicinity of U and in high concentrations, may react with it to produce uranium hydride (UH_3) (Eq. 2)[4,5]. Such reaction may be regarded as unwanted since uranium hydride behaves pyrophorically under sudden exposure to air and under certain conditions (large quantity and high surface area)[6].

$$U + 2H_2O \rightarrow UO_2 + 2H_2 \quad (1)$$

$$2U + 3H_2 \rightarrow 2UH_3 \quad (2)$$

There has been an ongoing controversy between different research groups on whether the solid corrosion products arising will contain UH_3[4,5,7–19] or not[20–23], in addition to UO_2, and if so, how much is likely to be present and in what distribution.

Recently, the kinetics of the uranium-water corrosion reaction was examined under immersed and contained conditions for prolonged periods (up to ~60 days)[4,5]. Analysis of the long-duration experiments showed that under certain conditions bulk-UH_3 formation can and will occur on a uranium sample. The parameters affecting the quantity of UH_3 forming in such a system were also verified[4,5]. It was found that the ratio of UH_3 to the oxide corrosion products decreased as the reaction period and temperature of reaction increased. The parameters affecting the location of the hydrides and hydriding behaviour of the metal were also examined[24–27]. The abundance of water in the uranium-water-hydrogen system has led us to assume that an additional corrosion process is occurring among others in this complex ternary system, the oxidation of UH_3 with water[4,5]. This reaction is a highly favourable process as it turns pyrophoric UH_3 to UO_2, which, depending on surface area may be considered less reactive.

There is only a limited amount of literature available on the oxidation of UH_3 with water[11,22,28–35]. According to the literature, the oxidation proceeds through the following exothermic reaction:

University of Bristol, Interface Analysis Centre, School of Physics, HH Wills Physics Laboratory, Tyndall Avenue, Bristol, BS8 1TL, United Kingdom. ✉e-mail: antonisbanos@gmail.com

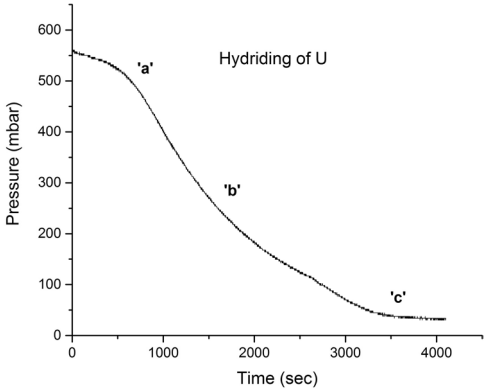

Figure 1. Hydriding of Magnox-U at 240 °C, 550 mbar H_2.

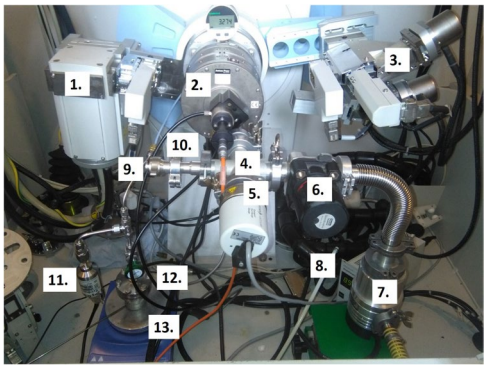

Figure 2. Experimental set-up developed for hot-stage X-ray diffraction (XRD) hydriding analysis. The set-up is composed of: (1) X-ray tube; (2) HTK 1200 high temperature oven chamber; (3) X-ray detector (receiving side); (4) 22 mm pipe cross-piece; (5) Full range pressure gauge; (6) Speed valve; (7) Turbo pump (backed-up by a roughing pump); 8) Full range gauge controller and digital display; (9) Bleed-valve; (10) Fitted high temperature sample stage; 11) 0 - 6895 mbar pressure transducer; (12) Source hydrogen) bed; (13) High temperature hot-plate.

$$2UH_3 + 4H_2O \rightarrow 2UO_2 + 7H_2 \quad (3)$$

The reaction kinetics of UH_3 with water vapour and liquid water are regarded to be the same[33,34]. Through the reaction of 0.2–1 g of UH_3 with liquid water, Beethan *et al.*[30] observed bubbles, ascribed to H_2, being released to the water. The reaction was very rapid initially and slowed after 2–5 h. Spedding *et al.*[31] found that the sample mass to water ratio played an important role in the reaction, with small amounts of water only reacting with UH_3 regionally and not self-sustaining the reaction. Baker *et al.*[11] reacted UH_3 with water vapour and observed the kinetics to decrease after an early accelerating stage, consuming 15–20% of the hydride after two weeks of reaction at environmental conditions. The reaction only reached 83% of completion at 100 °C, under saturated conditions, suggesting that the reaction kinetics slow to an almost negligible rate. Baker's findings were verified in a recent work by Goddard *et al.*[33,34], who observed this same termination stage after 80–90% of the sample was consumed.

There are a number of parameters affecting the reaction kinetics and also the extent of UH_3 oxidation. Baker *et al.*[11] found that the extent of UH_3 transformation to UO_2 was significantly increased with increasing temperature. Beetham suggested that water vapour pressure has a $P^{0.2\text{-}0.6}$ dependence with the rate, while Goddard *et al.*[33,34], after extrapolation of the rate to condensation conditions, suggested a square root dependence. However, the fraction of UH_3 reacted with water to form oxide was found to decrease with increasing water vapour pressure[11]. The temperature of UH_3 formation greatly affected the kinetics of UH_3 oxidation[33,34], with low temperatures of hydride formation resulting in subsequently enhanced oxidation kinetics[33,34], meaning the hydride material was more reactive. Finally, oxygen additions in water vapour were observed to accelerate the reaction[32–34], which is in direct contrast to what is well observed for the uranium-water reaction[19,21,23,36–43].

In this work, the reaction of UH_3 powder with water vapour under saturated environmental conditions will be examined. These conditions are most relevant to storage conditions at Sellafield. Two types of water vapour will be used for the reactions, normal de-ionised/purified water and 'heavy' water (D_2O). Analysis of the evolved gases will be performed using residual gas analysis to better understand the oxidation mechanism operating in the system.

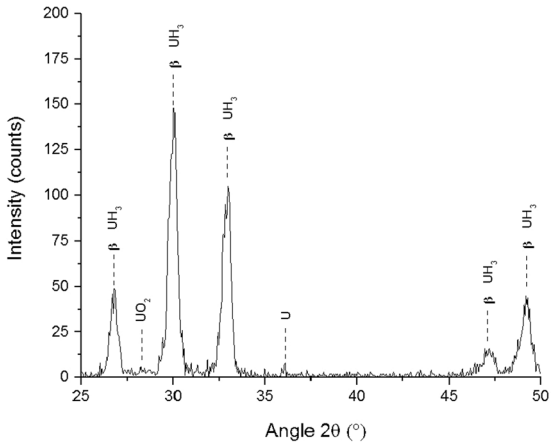

Figure 3. Raw X-ray diffraction (XRD) spectra for a reference sample hydriding at 240 °C, 500 mbar H_2. The analysis was performed with a Cu K_α source at 8 keV, between 25 and 50 ° angle 2θ, 0.05 step and 5 sec dwell time.

Results

***In-situ* UH_3 formation and analysis by hot-stage XRD.** The X-ray diffractometer, with the built-in gas rig (Fig. 2), was employed to hydride the surface of the sample *in-situ* and determine the chemical phase transformation occurring on the surface of the metal. Identical conditions were used for surface hydriding as for the experiment described in Section 1.2.2. The analysis was conducted to mimic the conditions of the reaction cell, producing newly-formed UH_3, and then immediately characterising it prior to any measurable oxidation. Preparation elsewhere and then transfer to the XRD would have resulted in a deleterious exposure of the hydride to air; hence this was the only possible experimental approach. No crystallite or particle size measurements were conducted since transformation of uranium was only occurring on the surface and analysis was only performed to confirm that UH_3 was formed. During hydrogen exposure of the metal sample, the XRD continually probed the sample and after the first UH_3 intensity peak was observed the reaction was halted and the cell volume evacuated. Subsequent detailed XRD analysis was performed under vacuum using a Cu K_α source between 25–50 ° 2θ with 0.05 ° steps and five second dwell time. Figure 3 illustrates the XRD spectra recorded after hydride formation (formed at 500 mbar of H_2, 240 °C). A thick hydride layer was formed on the surface (linear reaction stage - reaction front formation) since the XRD spectra showed only the five main hydride peaks.

Surface area analysis. The surface area of the sample was found to be ~1 $m^2.g^{-1}$. In the literature, the reported surface area of UH_3 powder used in experimental studies has ranged from 0.3–1.7 $m^2.g^{-1}$ [11,44–49]. The surface area is considered to be mainly affected by three parameters, the temperature of formation, the mass of the sample and the number of hydriding cycles applied to the material. The surface value of this work was higher than Totemeier *et al.*[46] who calculated a surface area of 0.5–1 $m^2.g^{-1}$ and lower than from Goddard *et al.*[33] who measured a surface are of 1.24 $m^2.g^{-1}$ (temperature of formation 80 °C).

Reaction rate determination. As the experimental cells has been thoroughly leak tested prior to the experiment, any observed pressure increase in the cell headspace, over time, was solely ascribed to H_2 gas generation from the oxidation of UH_3, according to Eq. (3). The measured pressure was converted to moles of produced H_2 gas using the ideal gas law through Eq. (4):

$$\boldsymbol{n}_{H_2} = (\boldsymbol{P}_{H_2}\boldsymbol{V})/(\boldsymbol{R}\,\boldsymbol{T}) \tag{4}$$

where P_{H2} (converted in atm) is the measured pressure of H_2 gas, V (in L) is the volume of the system, R is the ideal gas constant and has the value 0.082057 L. atm. mol^{-1}. K^{-1} and T (in K) is the temperature of the cell. Through Eq. (3), the moles of generated H_2 were then converted to milligrams of reacted UH_3. If complete conversion of UH_3 was assumed from Eq. (3), a theoretical expected value of mg UH_3 could be derived for each experiment. Subsequently the complete temporal data set was processed to calculate and plot the reaction rate as a function of increasing time from the onset of oxidation. The reaction rate was presented as the percentage conversion of UH_3 to UO_2 per unit time (mg of $_{reacted}$ UH_3.$mg_{theoretical}$ $UH_3{}^{-1}$.h^{-1}).

$UH_3 + H_2O$ experiment. A 2.2 g uranium hydride powder sample was reacted with water vapour under ambient conditions (~25 °C, ~31 mbar H_2O) in this experiment. Figure 4a,b illustrate the raw pressure generation data over time and the arising reaction plot, respectively. After non-linear fitting it was found that the reaction line profile could be expressed adequately by the classical Freundlich model as in Eq. (5):

$$\boldsymbol{y} = \boldsymbol{a}\boldsymbol{x}^{\boldsymbol{b}} \tag{5}$$

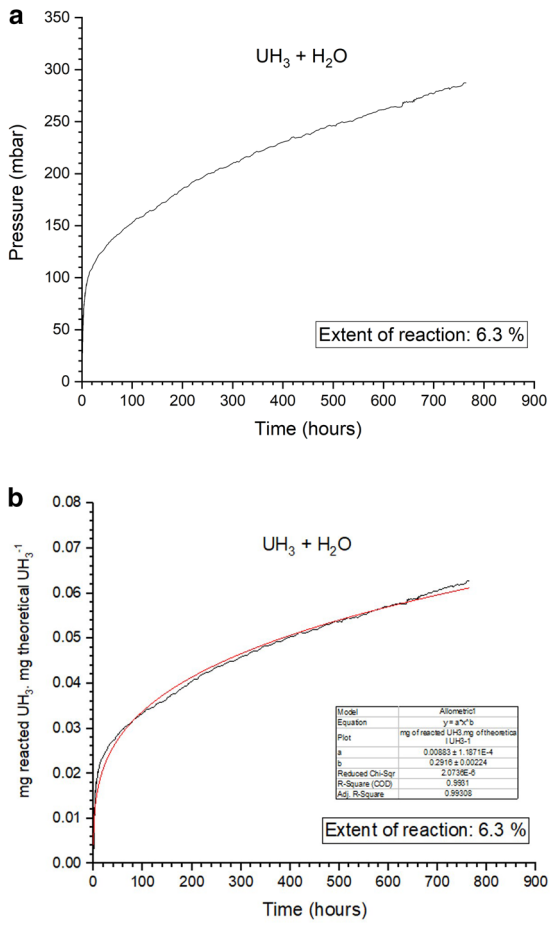

Figure 4. The oxidation of UH_3 with H_2O vapour for ambient conditions (25 °C, 31 mbar H_2O). On (**a**) the raw pressure generation data over time are displayed and on (**b**) the rate is defined as the proportion of the total UH_3 reacted to the theoretical of 2227.9 mg of UH_3 over time.

with a= 0.0088 being a coefficient and b= 0.2916 being the power of x. The Freundlich model generally represents the isothermal variation of adsorption of a quantity of gas adsorbed by unit mass of solid adsorbent with pressure[50]. It can also represent the amount absorbed per unit mass of absorbate. Here, the formula revealed that the rate of conversion of UH_3 to UO_2 was initially very robust and was governed by how fast water was adsorbing in the surface to react with 'fresh and non-oxidised hydride. The conversion rate continues to drop significantly over time with the UH_3 particles following a 'shrinking core' oxidation model where the UH_3 core is becoming smaller in size due to reaction over time. Uranium oxide acts as a protective layer which inhibits diffusion of the reactive agents to reach the oxide-hydride interface. This latter effect combined to the reduction of the reaction surface area govern the reaction kinetics at this later stage. Over a ~764-hour time period 6.3% of the starting UH_3 mass had been converted to UO_2, which marked the maximum extent of the reaction.

$UH_3 + D_2O$ experiment. A 1.2 g powder sample was prepared and reacted for this second experiment. Figure 5a,b show the derived pressure data and the corrosion progression over time for UH_3 oxidizing with saturated D_2O vapour at ~25 °C. The same behaviour was observed here as for the sample of the $UH_3 + H_2O$ experiment. The reaction rate line profile also obeyed to Eq. (5) with the following parameters being derived from non-linear fitting:

a = 0.0089 being a coefficient and b = 0.3408.

The percentage extent of UH_3 transformation was ~10% for 1204 h of oxidation.

Reaction rate comparison. The two arising data sets showed very similar behaviours and the derived rates were very closely comparable. Table 1 integrates some of the parameters from both experiments. The rates were found to switch from the early initial robust stage to a gradual decelerating stage at ~41.1 h and ~43.5 h for $UH_3 + H_2O$ and $UH_3 + D_2O$, respectively. The rate of the H_2O experiment at this stage was ~44% slower than the one of the D_2O experiment. The reaction period between the two experiments was very different since the H_2O experiment was stopped after 763 h and the D_2O experiment after 1204 h. This affected the extent of the reaction which also varied between the experiments (H_2O experiment = 6.3%, D_2O experiment = 10%). Of course, the extent of reaction could also be affected by the rate of conversion/reaction. To compare the reaction kinetics between the experiments, the conversion rate was calculated at a random point by using Eq. (5). For a selected value of x=

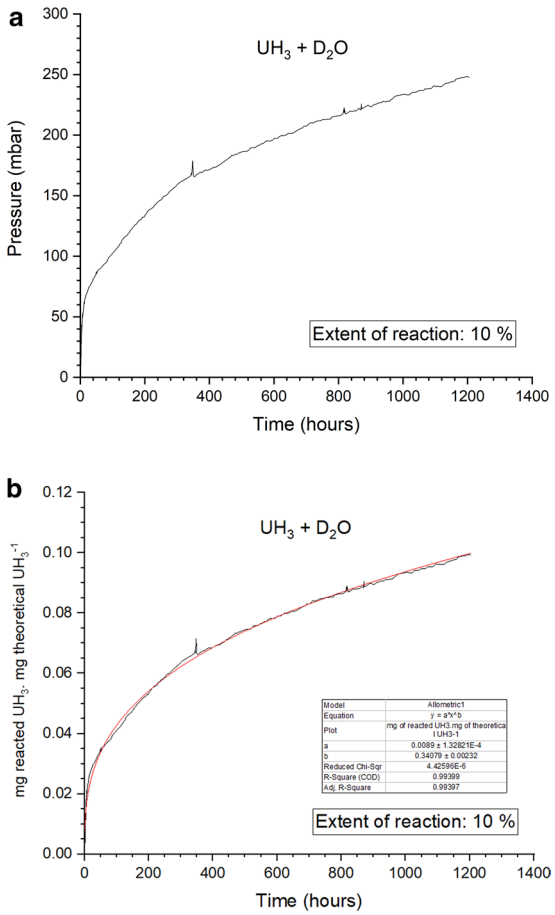

Figure 5. The oxidation of UH_3 with D_2O vapour for ambient conditions (25 °C, 31 mbar D_2O). On (**a**) the raw pressure generation data over time are displayed and on (**b**) the rate is defined as the proportion of the total UH_3 reacted to the theoretical of 1215.4 mg of UH_3, over time.

Experiment	Sample mass (g)	Reaction period (hours)	$y = ax^b$	Reaction rate k -at 600 h ($mg_{of\ reacted}\ UH_3.mg_{theoretical}\ UH_3^{-1}.h^{-1}$)	Extent of reaction (%)
$UH_3 + H_2O$	2.2	~764	a=0.0088, b=0.2916	0.000095	~6.3
$UH_3 + D_2O$	1.2	~1204	a= 0.0089, b= 0.3408	0.000131	~10

Table 1. The parameters of the $UH_3 + H_2O$ and $UH_3 + D_2O$ experiments.

time= 600 h, the reaction rate was 0.000095 and 0.000131 $mg_{of\ reacted}\ UH_3.mg_{theoretical}\ UH_3^{-1}.h^{-1}$ for the $UH_3 + H_2O$ and $UH_3 + D_2O$ systems, respectively. Thus, the conversion rate was 38.55% faster on the D_2O experiment when compared to the H_2O experiment.

In the literature, there was only a limited amount of work reporting the kinetics of this reaction, especially in such a low temperature regime. Baker *et al.*[11] reported 15–20% of UH_3 conversion to UO_2 for a 336 h oxidation time period. Based on the reaction extent, the kinetics were considerably faster in comparison to this work, since for the H_2O and D_2O experiments only 4.8% and 6.6% of the hydride reacted over the first 336-hour period. Goddard *et al.*[33] used TGA analysis to examine the oxidation reaction of UH_3 over a wide range of temperatures with water and water vapour. They observed the reaction of UH_3 prepared at 80 °C, oxidising at 30 °C, over saturated conditions. For such a hydride formation temperature (80 °C), the production of both α-UH_3 and β-UH_3 would be expected[51,52]. Owing to the different expected reactivity between α-UH_3 and β-UH_3 with water they yielded two different rates, one for each component. Through comparison of the reported rate from oxidation of the β-UH_3 component at 30 °C, it was found that the quasi-linear rate of 0.0004 $mg_{reacted}\ UH_3.mg_{theoretical}UH_3^{-1}.h^{-1}$ which was suggested in that work is lower than those determined in this work.

Residual gas analysis. RGA analysis of the evolved gases was conducted periodically to gain a closer insight into the corrosion mechanism of UH_3 oxidation. The method of analysis was described in Section 1.2.5.2. The results from gas analysis on the $UH_3 + H_2O$ system showed almost solely H_2 gas generating in the headspace.

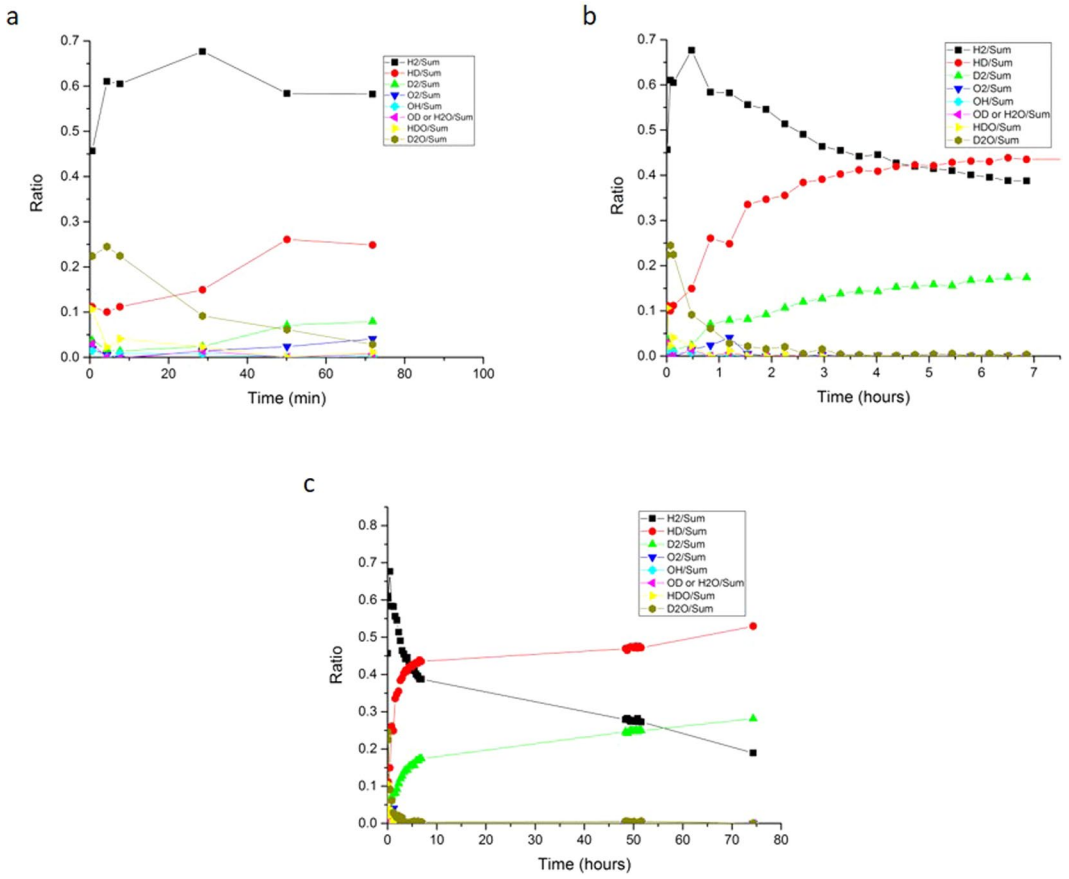

Figure 6. Ratio profile of the relative gas pressure of the evolved gases from oxidation reaction of UH_3 with D_2O for (**a**) 1 h (**b**) 7 h of oxidation and (**c**) 75 h of reaction.

Insignificant amounts of H_2O were also detected. However, not much information about the mechanism of the reaction could be drawn since origination of H^+ ions could not be resolved, between the UH_3 and H_2O. Using isotopic labelling of the water, the path of D^+ ions derived from water and H^+ ions from UH_3 could be traced and the mechanism of oxidation could be verified. For $UH_3 + D_2O$, the headspace gas was analysed with an initial 20-min periodicity for the first 7 h of reaction. Gas sampling and analysis was then performed at ~50 h and ~75 h of reaction. As already explained in Section 1.2.5.2, at least 11 full scans were performed for each time interval where the sampling valve was opened. After background subtraction (blank experiment), the ratio of the relative gas pressure (detected as a specific mass in amu) to the overall gas pressure was derived. Figure 6a–c show the ratios of the detected gases over exposure time. H_2, HD, D_2, O_2 OH, H_2O or OD, HDO and D_2O were detected after background subtraction.

Over the first 30 min of oxidation, we observed a sudden increase in the H_2 gas ratio, concomitant with a decrease in the D_2O ratio and slight increase in the HD ratio (Fig. 6a). Following the first 30 min, the D_2O ratio drops to almost zero (background level). Apart from H_2, HD and D_2 ratios, all detected gas ratios fell to almost zero/background levels at this stage (Fig. 6b). Interestingly, the H_2 gas ratio starts to decrease simultaneous to an observed increase of HD and D_2 ratios (Fig. 6a,b). After this point, H_2 gas ratio continued to decrease and HD, D_2 ratios continued to increase parabolically until analysis was ceased (Fig. 6c).

Discussion

From both corrosion experiments, the measured rates from the quasi-linear decelerating regimes were consistently lower in comparison to the limited amount of data reported in the literature. As already discussed in the introduction the rate of the reaction, after the early initial stages of oxidation, is mainly affected by four different parameters, the temperature of reaction, the water vapour pressure, the temperature of UH_3 formation and oxygen additions. Higher temperature, higher water vapour pressure and higher oxygen additions would result in enhanced rate kinetics, contrary to the temperature of UH_3 formation where the effect is the inverse (higher formation temperature leads to decreased rate). In Baker's work[11], where the rate of reaction was significantly higher, the conditions of UH_3 formation were not stated in the paper. It is believed that the temperature of formation was lower than the one of this work or a potential leak could have accelerated the rate. Lower temperature of UH_3 preparation, combined with slightly higher temperature of UH_3 oxidation, were also responsible for the observed higher rate kinetics of Goddard's results[33]. One of the main findings of Goddard's work was the strong effect of temperature of UH_3 formation on the subsequent hydrolysis rate, with measured oxidation rates being one order

of magnitude higher for samples prepared at 50 °C, in comparison to those prepared at 160 °C. For the compared rate of that work, they prepared the UH_3 powder at 80 °C, which is considerably lower formation temperature than used in this present work (240 °C). This had a strong effect on the surface area which was higher (1.24 $m^2.g^{-1}$), in comparison to this work (~1 $m^2.g^{-1}$). The three repetitions of hydriding-dehydriding was expected to have resulted in small micron-scale particles with small expected crystallite size[40]. However, a minor possibility is that the relatively high temperature of formation may have resulted in potentially incomplete transformation over the first hydriding sessions. Furthermore, the temperature of dehydriding (500 °C) may have resulted in potential recrystallisation of the metallic particles when these were formed with some associated diffusion bonding between particles[53]. Thus, for our results where the rate was relatively lower, the results are considered reasonable. Additionally, the temperature of the reaction was 5 °C higher (30 °C) than the temperature of reaction used here.

It is not yet clear yet what causes such a drop in kinetics with increasing temperature of UH_3 formation. Goddard *et al.*[33] concluded that surface area and crystallite size cannot account for such a difference in the rate. However, if the phase of the hydride switches from α-hydride to β-hydride due to exothermic heating from oxidation, differences in the microstructural features between phases may lead to cracking of the particles, thereby increasing the reactive surface area and accelerating the measured kinetics of diffusion of the oxidising species[33].

RGA analysis in the $UH_3 + D_2O$ experiment provided a closer insight on the early stages of the reaction by tracking the path of D^+ ions in the gas phase. From this analysis, four observations were highlighted and interpreted:

i. **H_2 gas contribution dominated the overall gas pressure in the initial stages of oxidation**. This implied substantial transformation of UH_3 to UO_2 through Eq. (3); releasing H_2 as a by-product.
ii. **The presence of HD in the gas mixture**. Formation of this gas could only occur from combination of H^+ ions originating from UH_3 (breakage of the U-H bond) and D^+ ions originating from dissociation of water. Combination of the H^+ - D^+ ions would most likely occur at the hydride-oxide interface, where the H^+ ions are initially produced. Only through partial dissociation of water (OD^-D^+) and diffusion of an OD^- entity through the protective oxide, would it be possible for D^+ ions to reach the hydride-oxide interface and bond with H^+. Thus, OD^- is one (if not the only) oxidising entity in the system. It was not possible to arrive at any further conclusions with regards to the contribution of full dissociation (if any) with the available RGA data. Such a process cannot be excluded from the system. It was also not possible to determine whether HD was forming at the hydride-oxide interface or at the oxide-gas interface. In both instances UO_2 is a recognised catalyst and has been implicated previously as a reactive surface for gas dissociation and recombination[40].
iii. **The formation of D_2 in the gas reaction products verified the coupling of D^+ ions**. This coupling could potentially occur at the gas-oxide or the hydride-oxide interface where D^+ from dissociation of water or breakage of OD^- bond is observed, respectively. Comments from (ii) regarding catalytic behaviour of the oxide also apply.
iv. **The continuous decrease of H_2 ratio in the gas products, with increasing oxidation time**. This drop occurs simultaneous to the increase in the HD and D_2 ratios. Thus, the H_2 ratio profile line was interrelated with the HD and D_2 ratio profile lines. This was clearly observed over the entire course of measurement (Fig. 6a–c). In practice, this means that H^+ ions generated at the hydride-oxide interface will not only recombine with each other but will couple with generated D^+ ions from the breakage of the OD^- bond, at the hydride-oxide interface. The more H^+ coupled with D^+ ions, the less residual H^+ was present to couple with itself to form H_2. For the D_2 gas, this means that the gas is produced from both the bonding of D^+- D^+ ions at the hydride-oxide interface, but also from recombination of the same ions after partial (or full) dissociation of D_2O at the gas-oxide interface.

From the above, a mechanism for the oxidative corrosion of UH_3 with water vapour can be suggested. After newly-formed UH_3 is produced, very limited oxidation of the surface of the hydride particles is expected to occur over time, especially under UHV conditions. The heat of formation at this stage ranged from 385.4–387 kJ.mol^{-1} [28,29], which is significantly lower than that of the $UH_3 + O_2$ system. Once the oxide layer nucleates and covers the hydride particle, the reaction will follow a 'shrinking core' or 'contracting envelope' model[22,30,32–34]. This was indicated from the decelerated oxidation kinetics over time and the kinetic profile of the reaction (see Eq. (5) and section 1.2.3) Thus, the kinetics will depend on:

- The surface area/particle size of the hydride[33].
- The growth of the oxide which is controlled by the diffusion of the oxidising entities through the already formed oxide.

The same principles should apply on the gas-oxide interface between H_2O and UO_2, as described in the uranium-water oxidation. The presence of HD in the gas products (highlight (ii) above) implies that partial dissociation of D_2O occurs at the gas-oxide interface, according to the following equation:

$$\boldsymbol{D_2O \rightarrow D^+ + OD^-} \tag{6}$$

Full dissociation ($2D^+$ - O^{2-}) cannot be excluded from the process, even though partial dissociation should be the dominant process, according to the derived percentage ratios of HD and D_2 on the generated gases ($HD_{ratio} > D_{2ratio}$). Allen *et al.*[36] also confirmed the suggestion of a singly charged ion (OD^-) as the dominating diffusing entity by measuring the difference in the activation energy between uranium and water vapour (38 kJ.mol^{-1}) and uranium with oxygen (76.57 kJ.mol^{-1}). At the hydride-oxide interface three processes will occur:

$$UH_3 \rightarrow U + 3e^- + 3H^+ \quad (7)$$

$$U \rightarrow U^{4+} + 4e^- \quad (8)$$

$$OD^- \rightarrow O^{2-} + D^+ \quad (9)$$

Formation of UO_2 occurs through the following reaction:

$$U^{4+} + 2\,O^{2-} \rightarrow UO_2 \quad (10)$$

Three combinations are then possible for the generated H^+ and D^+ ions at the hydride-oxide interface. H^+ ions from Eq. (7) could couple with each other to form H_2 gas and diffuse out to the headspace as follows:

$$H^+ + H^+ + 2e^- \rightarrow H_{2(g)} \quad (11)$$

or couple with the D^+ produced from Eq. (9) to form HD gas as follows:

$$H^+ + D^+ + 2e^- \rightarrow HD_{(g)} \quad (12)$$

It is believed that these two processes are the dominating ones at the hydride-oxide interface. D_2 formation occurs at the hydride-oxide interface but also at the gas-oxide interface through the same process:

$$D^+ + D^+ + 2e^- \rightarrow D_{2(g)} \quad (13)$$

with electrons produced at the hydride-oxide interface, partially migrating through the oxide (electron tunnelling) to the gas-oxide interface or incident radiation activating the UO_2 (as a semi-conductor with 2.2 eV band gap) to create reactive electron hole pairs.

One significant finding of this work was that oxidation of UH_3 at this temperature and pressure remains incomplete, with the extent of oxidation being ~10% after ~50 days of reaction ($UH_3 + D_2O$ experiment). Baker *et al.*[11] reported a 15–20% of reaction after 14 days at the same conditions, before the rate switches to almost zero kinetics. Goddard *et al.*[33], reported 27% of UH_3 conversion after ~20 days of reaction at 22 °C and before the rate slows down considerably. From the same work, with liquid water a ~23% reaction extent was also reported at 30 °C of reaction. Despite the discrepancy in the amount of remaining hydride between studies, this observation of substantial residual hydride after prolonged oxidation in water, ascribed to the forming surface oxide performing as a 'protective blanket' and isolating the hydride from further reaction. Under retrieval conditions, breakage of this protective oxide when handling the waste material may trigger a thermal excursion if a substantial bulk mass of UH_3 becomes exposed to air. In a worst-case scenario (which is highly unlikely) this exothermic phenomenon could reach sufficient temperature to release entrapped volatile fission products, expel fine uranium particles and ignite other flammable materials in the wasteform e.g. magnesium metal. Thus, understanding the conditions under which the material was kept over time, predicting the mass of bulk-UH_3 formed and then foreseeing the extent that this hydride was oxidised, is highly critical in classifying the risk that a certain batch of ILW may present during retrieval, repackaging, storage or disposal. These results show that bulk-UH_3 (if initially formed) may still be present in the corroding material after prolonged periods and further confirms the earlier synchrotron work published by Stitt *et al*. who demonstrated the persistence of bulk hydride in a cemented simulant waste form[54].

In this work, we have examined the oxidation kinetics of UH_3 powder with water vapour at 25 °C, under saturated conditions. Two experiments were conducted, one with H_2O and one with D_2O. RGA analysis of the evolved gases allowed us to gain greater insight into the mechanism of the reaction. From the analysis, it was found that:

i. The kinetics of the reaction show initially robust and continuously decelerating kinetics. This behaviour is indicative of a 'shrinking core' or 'contracting envelope' type oxidation behaviour.
ii. The kinetics of the quasi-linear decelerating stage were observed to be quite low compared to other works. This was attributed to the formation temperature of the UH_3 and U particles, respectively (high temperature of UH_3 formation 240 °C - high dehydriding temperature 500 °C) leading to lower surface area for the UH_3 powder and potential recrystallisation of the U particles[53].
iii. The extent of reaction/conversion of UH_3 was observed to be low: 6.6% after ~32 days for the $UH_3 + H_2O$ experiment and ~10% after ~50 days for the $UH_3 + D_2O$ experiment. This provides new evidence to bolster the case for the possible long duration persistence of UH_3 in legacy wastes.
iv. A mechanism for the reaction was suggested by interpreting the gas analysis data from the $UH_3 + D_2O$ experiment. The data implicates OH^- as the specie with primary responsibility for oxidation, with an associated implication that water vapour is adsorbed and dissociates on the outmost surface of the UO_2.

Methods

Sample preparation. Four uranium metal samples cut from the same parent Magnox-U coupon were used as the precursor material for this work. Extensive characterisation of the samples can be found in[24–27]. The bulk samples were mechanically abraded on all faces using SiC paper (P600) to remove surface grown oxide. One sample was sent to an X-ray diffractometer for surface hydriding *in-situ* using a hot-stage. The remaining three

metallic samples were turned to a UH_3 powder through a standard three-step hydriding-dehydriding process which will be described in the following section. Each sample was reacted separately in a sealed stainless-steel cell, and the UH_3 powder was prepared under the same pressure-temperature conditions (P = 500 mbar, T = 240 °C) in each case to ensure the consistency of the product materials. Powder preparation was not conducted for each sample at the same time, but only prior to any preliminary analysis or oxidation reaction. One out of the three powder samples was sent for BET surface area analysis, while the other two were used for corrosion reactions. Powdered samples prepared for the oxidation reactions remained in the same reaction cell where the hydriding-dehydriding preparation took place under high dynamic vacuum (1×10^{-6} mbar), prior to water vapour introduction. This ensured that no (or only negligible) oxidation would occur on the surface of the newly formed UH_3 powder. A more detailed description of the experimental procedure will be provided in Section 1.3.4.

UH_3 powder preparation (Hydriding - Dehydriding session). Each bulk uranium sample was placed in a sealed steel cell and connected to a gas control rig. The cell was evacuated down to 1×10^{-7} mbar and the temperature increased to 125 °C, while under dynamic vacuum. The sample was left to degas for ~16 h to drive off any adsorbed water. After degassing, the temperature was raised and left to stabilise at 240 °C. This temperature was regarded as ideal for fast phase transformation of the bulk metal sample to hydride powder. It should be noted that only β-UH_3 is produced at this temperature[52,55,56]. The sample volume was then introduced to 500 mbar of H_2 gas. The gas was provided by BOC and was stored in a $LaNi_5$ bed to further improve purity. Hydriding initiation was observed to occur after a defined induction period (point 'a' in Fig. 1). Figure 1 shows the first hydriding session for the sample used for surface area analysis. In the plot, the pressure drop owing to gas absorption by the metal can be observed on 'a'. After the passing of the accelerating, quasi-linear and decelerating stages of hydride formation (point 'b' on Fig. 1), the gas profile line plateaued (point 'c' on Fig. 1), signifying that the reaction had completed.

The remaining headspace gas was then fully evacuated and the cell volume isolated and the temperature raised to 500 °C. At this temperature, the hydride powder converts rapidly back to uranium (as a powder) with an associated pressure increase, ascribed to H_2 gas generation. After no further pressure increase was detected, indicating complete dehydriding of the sample, the volume was evacuated again. The first hydriding-dehydriding session was complete and the temperature was set to 240 °C for re-hydriding of the uranium powder using fresh H_2 gas. The hydriding-dehydriding cycle was repeated two additional times (three-times in total), preceding the final hydride oxidation experiments. This was done for two main reasons:

i. Non-complete UH_3 transformation was observed by other investigators after a single cycle of hydriding of uranium under similar conditions[57].
ii. Negligible change in the surface area of uranium between hydriding-dehydriding reactions was only observed after three hydriding-dehydriding cycles[58].

Hence, with the preparation above, complete uranium transformation to UH_3 is expected to be achieved, producing a hydride powder (in each instance) with comparable particle size and surface area.

Reaction water vapour. Two types of water were used for the oxidising experiments, deionised water for the $UH_3 + H_2O$ experiment and deuterated water (D_2O) for the $UH_3 + D_2O$ system. D_2O was provided by ACROS Organics. Both water beds followed a three-stage freeze-vacuum-melt process.

Experimental method. Two corrosion experiments were conducted in this work, UH_3 oxidation with normal water vapour (H_2O) and another with deuterated water vapour (D_2O), both under ambient saturated conditions. An identical experimental process was followed for both systems, with the only difference being the source of water providing the oxidising species into the reaction volume (from a bed). Once the UH_3 powder was prepared (end of 4th hydriding session), the furnace was switched off and the cell was left to cool down to ambient temperature conditions under high dynamic vacuum ($<1 \times 10^{-7}$ mbar). The reaction/working volume was then isolated from the turbo-pump and the source water bed was opened for water vapour to be admitted to the cell. Pressure and temperature in the cell were logged every second. Gas composition in the cell was also continually logged using an RGA system (MKS E-Vision instrument). Through the use of isotopically labelled water and by analysing the gases from the start of the reaction, information about the mechanism of the reaction could be derived.

Analysis techniques. *BET surface area analysis and XRD analysis.* The sample prepared for surface area analysis was sealed and transferred to the BET instrument for measurement. Analysis was performed by making a full 10-point adsorption-desorption isotherm. *In-situ* surface hydriding of the bulk metal was performed using hot-stage XRD to verify that uranium would reliably transform to UH_3 under the same hydriding conditions used in the gas control rig to make the hydride powder (240 °C, 500 mbar H_2). The hot-stage XRD set-up is shown in Fig. 2.

RGA analysis. RGA analysis of the evolved gases was performed for both oxidation experiments. The RGA analyser was setup only to periodically sample the headspace volume of the cell, by the opening and closing of an automated leak valve. Using an automated valve ensured the same leak magnitude was repeated at every sampling point. The valve was set to open with a 20-min time interval over the first 7 h of reaction. The overall sampling time-period, defined as the period needed for the valve to complete a full opening and closing was ~106 sec. The RGA was set to operate in bar chart mode between 1–50 atomic mass units (amu). The overall time needed for one complete scan was 9 sec. Thus, at least 11 full scans were performed each time the valve was opened. Owing

to the very robust and complex nature of the reaction at the early initial stage, the time interval under which gas sampling and analysis was performed was relatively high (t = 20 min). It was imperative that gas evolution over the initial accelerating reaction stage was analysed and recorded, since at this stage of the reaction the mechanism could be verified. Such frequent gas analysis was only performed over the first 7 h of reaction. After the reaction was switched to the quasi-linear decelerating stage, gas analysis was arbitrarily chosen to be performed at ~50 h and ~75 h.

'Blank' tests with absence of the uranium powder have been performed to identify if there was any interactions between the water and the stainless steel walls leading to H_2 formation. Negligible formation of H_2 has been detected over a long period during the blank tests and was subtracted from our results. Through the use of isotopically labelled water and by analysing the gases at the early initial stages, information about the mechanism of the reaction could be derived.

Data availability

The datasets generated during and/or analysed during the current study are available from the corresponding author on reasonable request.

Received: 16 September 2019; Accepted: 18 May 2020;
Published online: 11 June 2020

References

1. Sellafield ltd, Sellafield Plan, LD215 Issue 1 (August 2011). at, https://www.cumbria.gov.uk/eLibrary/Content/Internet/538/755/1929/17716/17720/17722/41333114920.pdf
2. The 2013 UK radioactive waste inventory. Nuclear decommissioning authority (NDA) URN 14D040 NDA/ST/STY(14)0011, (2014).
3. Sellafield ltd, ILW treatment and storage. (archived 2017). at, https://webarchive.nationalarchives.gov.uk/20170712123747/http://www.sellafieldsites.com/solution/waste-management/ilw-treatment-and-storage/.
4. Banos, A., Hallam, K. R. & Scott, T. Corrosion of uranium in liquid water under vacuum contained conditions. Part 1: The initial binary U + H2O(l) system. *Corrosion Science* **152**, 249–260 (2019).
5. Banos, A., Hallam, K. R. & Scott, T. Corrosion of uranium in liquid water under contained conditions with a headspace deuterium overpressure. Part 2: The ternary U + H2O(l) + D2 system. *Corrosion Science* **152**, 261–270 (2019).
6. Banos, A., Harker, N. & Scott, T. A review of uranium corrosion by hydrogen and the formation of uranium hydride. *Corrosion Science* **136**, 129–147, https://doi.org/10.1016/j.corsci.2018.03.002 (2018).
7. Frank, J.W. & Roebuck, A.H. Crevice corrosion of uranium and uranium alloys (No. ANL-5380). (Argonne National Lab., Lemont, Ill., 1955).
8. Draley, J. & Ruther, W. Some unusual effects of hydrogen in corrosion reactions. *Journal of The Electrochemical Society* **104**, 329–333 (1957).
9. Hopkinson, B. Kinetics of the uranium-steam reaction. *Journal of the Electrochemical Society* **106**, 102–106 (1959).
10. Kondo, T., Verink, E., Beck, F. & Fontana, M. Gas chromatographic and gravimetric studies of uranium oxidation mechanism. *Corrosion* **20**, 314t–320t (1964).
11. Baker, M. M., Less, L. & Orman, S. Uranium + water reaction. Part 1. - Kinetics, products and mechanism. Transactions of the Faraday. *Society* **62**, 2513–2524 (1966).
12. Kondo, T., Beck, F. & Fontana, M. A Gas chromatographic study on the kinetics of uranium oxidation in moist Environments. *Corrosion* **30**, 330–341 (1974).
13. Bennett, M., Myatt, B., Silvester, D. & Antill, J. The oxidation behaviour of uranium in air at 50–300 °C. *Journal of Nuclear Materials* **57**, 221–236 (1975).
14. Winer, K., Colmenares, C., Smith, R. & Wooten, F. Interaction of water vapor with clean and oxygen-covered uranium surfaces. *Surface Science* **183**, 67–99 (1987).
15. Marschman, S. C., Pyecha, T. & Abrefah, J. Metallographic examination of damaged N reactor spent nuclear fuel element SFEC5, 4378. (Pacific Northwest Lab., Richland, WA (United States), 1997).
16. Abrefah, J. & Sell, R. L. Oxidation of K-west basin spent nuclear fuel in moist helium atmosphere. (Pacific Northwest National Lab., Richland, WA (US), 1999).
17. Totemeier, T. C., Pahl, R. G. & Frank, S. M. Oxidation kinetics of hydride-bearing uranium metal corrosion products. *Journal of nuclear materials* **265**, 308–320 (1999).
18. Danon, A., Koresh, J. & Mintz, M. Temperature programmed desorption characterization of oxidized uranium surfaces: Relation to some gas-uranium reactions. *Langmuir* **15**, 5913–5920 (1999).
19. Delegard, C. H. & Schmidt, A. J. Uranium metal reaction behavior in water, sludge, and grout matrices. (Pacific Northwest National Laboratory, 2008).
20. Waber, J. A review of the corrosion behavior of uranium. (Los Alamos Scientific Lab., N. Mex., 1956).
21. Colmenares, C., Howell, R. & McCreary, T. Oxidation of uranium studied by gravimetric and positron annihilation techniques. (Lawrence Livermore National Lab., CA (USA), 1981).
22. Haschke, J. M. Reactions of plutonium and uranium with water: kinetics and potential hazards. (Los Alamos National Laboratory, 1995).
23. Kaminski, M. Batch Tests with unirradiated uranium metal fuel program report. (Argonne National Lab., IL (US), 2002).
24. Banos, A. Investigation of uranium corrosion in mixed water - hydrogen environments. PhD Thesis, University of Bristol, (2017).
25. Banos, A., Jones, C. & Scott, T. The effect of work-hardening and thermal annealing on the early stages of the uranium-hydrogen corrosion reaction. *Corrosion Science* **131**, 147–155 (2018).
26. Banos, A. & Scott, T. B. Statistical analysis of UH3 initiation using electron back-scattered diffraction (EBSD). *Solid State Ionics* **296**, 137–145, https://doi.org/10.1016/j.ssi.2016.09.018 (2016).
27. Banos, A., Stitt, C. & Scott, T. The effect of sample preparation on uranium hydriding. *Corrosion Science* **113**, 91–103 (2016).
28. Loscoe, P. Transitioning metallic uranium spent nuclear fuel from wet to dry storage. Waste Management Conference (2000).
29. Grenthe, I. *et al*. Chemical thermodynamics of uranium. Vol. 1 at, http://www.tdb.nea.fr/dbtdb/pubs/uranium.pdf (North-Holland Amsterdam, 1992).
30. Beetham, S. Uranium hydride stability trials. (AEA Technology report, 1995). Undocumented data reported by Goddard, D, Broan, C., Orr, R., Durham, P. & Woodhouse, G. Uranium hydride studies Part III: The kinetics of liquid water and water vapour reactions with uranium hydride. National Nuclear Lab., UK, (12545), 2013.
31. Spedding, F.H. *et al*. Uranium hydride; preparation, composition and physical properties. Nucleonics (US) Ceased publication Jan;4(1):4, https://www.ncbi.nlm.nih.gov/pubmed/18106041 (1949).

32. Punni, J. Uranium hydride passivation in oxidising environments at 30 °C. (1996). Undocumented data reported by Goddard, D., Broan, C., Orr, R., Durham, P. & Woodhouse, G. Uranium hydride studies Part III: The kinetics of liquid water and water vapour reactions with uranium hydride. National Nuclear Lab., UK, (12545), 2013.
33. Goddard, D., Broan, C., Orr, R., Durham, P. & Woodhouse, G. Uranium hydride studies Part III: The kinetics of liquid water and water vapour reactions with uranium hydride. National Nuclear Lab., UK, (12545) (2013).
34. Orr, R., Broan, C. & Goddard, D. Uranium hydride studies Part IV: Summary and conclusions. (National Nuclear Lab., UK (12546), 2013.
35. Gregson, P. & Gilchrist, P. The pyrophoricity of elemental uranium and uranium hydride. BNFL, (2003).
36. Allen, G. C., Tucker, P. M. & Lewis, R. A. X-ray photoelectron spectroscopy study of the initial oxidation of uranium metal in oxygen + water-vapour mixtures. *Journal of the Chemical Society, Faraday Transactions 2: Molecular and Chemical Physics* **80**, 991–1000 (1984).
37. Orman, S., Baker, M. M., Bleloch, J. & Less, N. Uranium compatibility studies. Part 3. The influence of oxygen on the uranium-water reaction. United Kingdom Atomic Energy Authority. Weapons Group. Atomic Weapons Research Establishment, Aldermaston, Berks, England, (1964).
38. Baker, M. M., Less, L. & Orman, S. Uranium + water reaction. Part 2. - Effect of oxygen and other gases. Transactions of the Faraday. *Society* **62**, 2525–2530 (1966).
39. Greenholt, C. J. & Weirick, L. J. The oxidation of uranium-0.75 wt% titanium in environments containing oxygen and/or water vapor at 140 °C. *Journal of Nuclear Materials* **144**, 110–120 (1987).
40. Harker, N. The corrosion of uranium in sealed environments containing oxygen and water vapour. PhD thesis, University of Bristol, (2012).
41. Corcoran, V. J., Johnston, C., Metcalfe, W. & Thorpe, J. The water vapour corrosion of uranium and its prevention. Atomic Weapons Research Establishment, Aldermaston (England), (1965).
42. McGillivray, G., Geeson, D. & Greenwood, R. Studies of the kinetics and mechanism of the oxidation of uranium by dry and moist air. A model for determining the oxidation rate over a wide range of temperatures and water vapour pressures. *Journal of Nuclear Materials* **208**, 81–97 (1994).
43. Jackson, R., Condon, J. & Steckel, L. Uranium/water vapor reactions in gaseous atmospheres. (Oak Ridge Y-12 Plant, TN (USA), 1977).
44. Wicke, E. & Otto, K. The uranium-hydrogen system and the kinetics of uranium hydride formation. Z. physik. Chem. (Frankfurt) 31 (1962).
45. Powell, G., Harper, W. & Kirkpatrick, J. The kinetics of the hydriding of uranium metal. *Journal of the Less Common Metals* **172**, 116–123 (1991).
46. Totemeier, T., Pahl, R., Hayes, S. & Frank, S. Characterization of corroded metallic uranium fuel plates. *Journal of Nuclear Materials* **256**, 87–95 (1998).
47. Longhurst, G. Pyrophoricity of Tritium-Storage Bed Materials a. *Fusion Science and Technology* **14**, 750–755 (1988).
48. Orr, R., Broan, C., Goddard, D., Woodhouse, G. & Durham, P. Uranium hydride studies Part II: Uranium hydride formation and characterisation. National Nuclear Lab., UK, (12544), 2013.
49. Alire, R., Mueller, B., Peterson, C. L. & Mosley, J. R. Reaction kinetics of uranium and deuterium. *The Journal of Chemical Physics* **52**, 37–46 (1970).
50. Freundlich, H. Kapillarchemie, eine Darstellung der Chemie der Kolloide und verwandter Gebiete. Akademische Verlagsgesellschaft, (1922).
51. Mulford, R., Ellinger, F. & Zachariasen, W. A new form of uranium hydride1. *Journal of the American Chemical Society* **76**, 297–298 (1954).
52. Abraham, B. & Flotow, H. The heats of formation of uranium hydride, uranium deuteride and uranium tritide at 25 °C. *Journal of the American Chemical Society* **77**, 1446–1448 (1955).
53. Bloch, J. & Mintz, M. H. The effect of thermal annealing on the hydriding kinetics of uranium. *Journal of the Less Common Metals* **166**, 241–251 (1990).
54. Stitt, C. *et al*. An Investigation on the persistence of uranium hydride during storage of simulant nuclear waste packages. *PloS one* **10**, e0132284 (2015).
55. Flotow, H. E., Lohr, H. R., Abraham, B. M. & Osborne, D. W. The heat capacity and thermodynamic functions of β-uranium hydride from 5 to 350 K. 1, 2. *Journal of the American Chemical Society* **81**, 3529–3533 (1959).
56. Bartscher, W. *et al*. Neutron diffraction study of β-UD3 and β-UH3. *Solid state communications* **53**, 423–426 (1985).
57. Sunwoo, A. & Goto, D. Effects of processing on microstructure and properties of α-uranium formed parts. *Scripta materialia* **47**, 261–266 (2002).
58. Bloch, J. The hydriding kinetics of activated uranium powder under low (near equilibrium) hydrogen pressure. *Journal of alloys and compounds* **361**, 130–137 (2003).

Acknowledgements

The authors would like to thank the Engineering and Physical Sciences Research Council (EPSRC) and Sellafield Ltd for funding this project as part of 42-month PhD research studentship (Ref: 1338575), at the Interface Analysis Centre (IAC), School of Physics, University of Bristol. We would also like to thank Mr John Jowsey and Dr Anna Adamska from the Sellafield Centre for Expertise in Uranium and Reactive Metals (URM) for contextual guidance and technical input.

Author contributions

A.B. prepared the figures, tables, experimental and methods. T.S. and A.B. prepared the introduction, results and discussion. Both authors reviewed multiple times the manuscript.

Competing interests

The authors declare no competing interests.

Additional information

Correspondence and requests for materials should be addressed to A.B.

Reprints and permissions information is available at www.nature.com/reprints.

Publisher's note Springer Nature remains neutral with regard to jurisdictional claims in published maps and institutional affiliations.